Left-handed optical torque on dipolar plasmonic nanoparticles induced by Fano-like resonance

Huajin Chen,[1,2,3] Lv Feng,[2] Jiangnan Ma,[2] Chenghua Liang,[1] Zhifang Lin,[3,4] and Hongxia Zheng[1,*]

[1]*School of Electronic Engineering, Guangxi University of Science and Technology, Liuzhou, Guangxi 545006, China*

[2]*School of Automation, Guangxi University of Science and Technology, Liuzhou, Guangxi 545006, China*

[3]*State Key Laboratory of Surface Physics and Department of Physics, Fudan University, Shanghai 200433, China*

[4]*Collaborative Innovation Center of Advanced Microstructures, Nanjing University, Nanjing 210093, China*

(Received 20 April 2022; revised 6 July 2022; accepted 13 July 2022; published 1 August 2022)

We theoretically and numerically demonstrate that Fano-like resonance can induce a left-handed optical torque on a dipolar plasmonic core-shell nanoparticle in the interference optical field composed of two linearly polarized plane waves. It is shown that the optical torque on the dipolar plasmonic nanoparticle is significantly enhanced at the Fano-like resonance, and its direction is opposite to that of the angular momentum of the incident field, termed Fano-like resonance-induced left-handed optical torque. The extinction spectra exhibit that the Fano-like resonance stems from the coupling between a narrow electric quadrupole dark mode and a broad electric dipole bright mode. In addition, such Fano-like resonance-induced left-handed optical torque can flexibly be tailored by the particle morphology. To further trace the physical origin of the left-handed optical torque, we derive an analytical expression of optical torques up to electric quadrupole in generic monochromatic optical fields based on the multipole expansion theory. The results obtained from our analytical expression show that the left-handed optical torque comes completely from the electric quadrupole terms while other terms from the electric dipole make no contribution. Our results may open a new avenue for tailoring optical torques on plasmonic structures.

DOI: 10.1103/PhysRevB.106.054301

I. INTRODUCTION

Light carries both linear and angular momenta, and as such it can exert an optical force and torque on matter due to the momenta exchange between light and matter [1–4]. Optical force is an excellent tool for manipulating microscopic particles, since it can push particles forward along the direction of light propagation [5–7], trap particles to the extremum of light intensity (now well-known as optical tweezers) [8–10], and even, pull particles toward light source, known as the concept of negative optical force [11–13]. Optical torque, the angular analog of optical force, which can spin or rotate trapped particles, add the degrees of freedom to particle manipulation, has attracted considerable attention in recent decades [14–22]. Intriguingly, similar to the counterintuitive phenomenon of negative optical force, negative optical torque can cause the rotation of objects opposite to the direction of the incident angular momentum [23,24], usually termed also as left-handed optical torque. Such left-handed optical torque was, both theoretically and experimentally, demonstrated via birefringent nanostructures immersed in circularly polarized Gaussian beams [25,26]. It was also proposed that the left-handed optical torque can rotate the bounded nanoparticle dimers in the direction reversed with respect to that of the incident circular polarization [27]. Left-handed optical torque was found on arrays of metal nanoparticles, and which is dependent on the number, separation and configuration of the arrays [28]. It was reported recently that chiral particles can also induce a left-handed optical torque illuminated by circularly polarized optical beams [18,29,30]. It is noted that the occurrence of the left-handed optical torque rely on size in the Mie regime, configuration, or constituent material of the particles, but little attention is focused on a single small particle such as a dipolar sphere. In addition, most of the above researches are based on the analytical theories within the dipole approximation to trace the underlying physics of optical torques [14–22,27–30]. However, these analytical methods may be invalid for some special cases where higher order multipoles excited in the particles make a significant contribution to the optical torques. Here we show that, a simple optical field composed of two interfering plane waves can exert a left-handed optical torque on a dipolar spherical nanoparticle by taking advantage of the so-called Fano-like resonance due to the coupling between multiple multipoles excited in the particle.

Fano resonance describes the coupling of a discrete atomic state with a continuum in the original work of Fano [31], while nowadays it is generally extended to a broader definition in which a narrow resonance is coupled to a broad resonant mode [32,33]. Such asymmetric Fano-like line shapes have been observed in a wide variety of systems, such as photonic crystals [34,35], metamaterials [32,36], and plasmonics [32,37]. Their unique properties can find extensive applications, including optical switching [38,39], surface enhanced Raman scattering [40,41], plasmon-induced transparency [42,43], and many others [44–46]. In particular, the effect of the Fano resonance on optical forces have been extensively explored in recent years [47–54]. However, its effect on tailoring the optical torque that plays a crucial role in optical manipulation, has yet to be explored.

In this paper, we show that a left-handed optical torque can be achieved for a dipolar Ag-Au core-shell sphere via exciting

*hxzheng18@fudan.edu.cn

 ©2022 American Physical Society

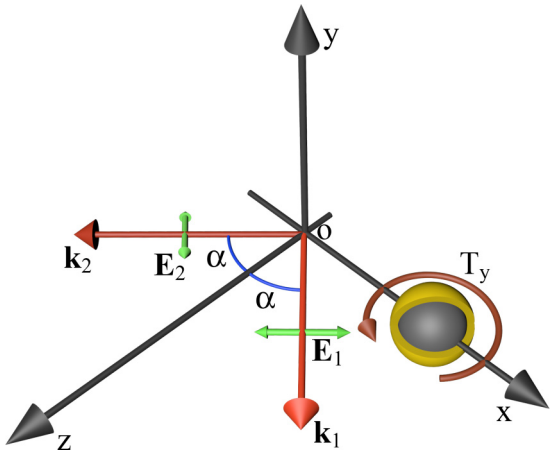

FIG. 1. Schematic illustration of an Ag-Au nanoparticle illuminated by the incident optical field composed of two interference plane waves symmetric with respect to z axis with the same incident angle $\alpha = 55^\circ$ on the xoz plane. Two plane waves share the same polarized vector $(p, q) = (1, 0)$, denoted by the double-headed arrows the orientations along which the electric fields are polarized. The particle has core radius $R_1 = 35$ nm and shell radius $R_2 = 43$ nm, which is supposed to be immersed in water and located at $x = 52$ nm.

its Fano-like resonance in two interfering plane waves with the same linear polarization. Such Fano-like resonance-induced left-handed optical torque can rotate the nanoparticle around its axis opposite to the direction of the incident angular momentum. Also, the left-handed optical torque can flexibly be tuned by adjusting the core and shell radii of the nanoparticle as well as the incident wavelength. The extinction spectra based on the Mie scattering theory reveal that Fano-like resonance arises from the interaction between a broad electric dipole mode and a narrow electric quadrupole one. It is noted that the electric quadrupole mode is usually difficult to be excited on a dipolar spherical particle. To further reveal the physical mechanism of the left-handed optical torque, the analytical expression of optical torques up to electric quadrupole in arbitrary free-space monochromatic optical fields is derived based on the multipole expansion theory. The analytical results exhibit that the left-handed optical torque is dominated by the electric quadrupole term while other terms from the electric dipole with their signs are always same with the one of the incident angular momentum. As a result, the analytical theory based on the dipole approximation generally used for dipolar particles is unavailable for our case. These findings provide an alternative way to realize the left-handed optical torque as well as deepen the physical understanding of light-matter interaction.

II. RESULTS AND DISCUSSION

To illustrate the Fano-like resonance-induced left-handed optical torque, we consider that a plasmonic Ag-Au core-shell spherical nanoparticle is illuminated by an optical field composed of two linearly polarized plane waves, as is schematically shown in Fig. 1. In experiment, the Ag-Au core-shell spherical nanoparticle can be synthesized by a simple chemical reduction technique [55]. The dielectric constants of Ag and Au can be theoretically derived by the Drude's dielectric function [56,57] $\varepsilon(\omega) = \varepsilon_\infty - \omega_p^2/(\omega^2 + i\omega\Gamma)$, where ε_∞ is the high-frequency-limit dielectric constant, ω_p is the plasmon resonance frequency, and Γ is the damping constant. In our calculations, we use the best experimental fit parameters as $\varepsilon_\infty = 4.039$, $\omega_p = 9.1721$ eV, and $\Gamma = 0.0207$ eV for Ag, while $\varepsilon_\infty = 8.7499$, $\omega_p = 9.0146$ eV, and $\Gamma = 0.0691$ eV for Au to obtain the dielectric constants [55]. The electric field of the incident optical field is given by

$$\mathbf{E}_{\rm inc} = \mathbf{E}_1 + \mathbf{E}_2, \quad \text{with } \mathbf{E}_j = E_0\, \boldsymbol{\mathcal{E}}_j\, e^{i k \hat{\mathbf{k}}_j \cdot \mathbf{r}}, \tag{1}$$

where k is the wave number in the background and $\hat{\mathbf{k}}_j = \cos\alpha\, \hat{\mathbf{z}} \pm \sin\alpha\, \hat{\mathbf{x}}$ for $j = 1, 2$ denotes the propagation direction of the jth plane wave. The complex polarization vectors $\boldsymbol{\mathcal{E}}_j$ are

$$\boldsymbol{\mathcal{E}}_j = p\, \hat{\boldsymbol{\theta}}_{k_j} + q\, \hat{\boldsymbol{\phi}}_{k_j} \quad \text{for } j = 1, 2, \tag{2}$$

where $\hat{\boldsymbol{\theta}}_{k_j}$ and $\hat{\boldsymbol{\phi}}_{k_j}$ denote, respectively, the directions of increasing polar angle and azimuthal angle in spherical coordinate system for the jth wave vector. In our case, two waves share the same polarized vector $(p, q) = (1, 0)$, perpendicular to both the wave vector of the jth plane wave as well as y axis. The time dependence $e^{-i\omega t}$ is assumed and suppressed throughout the paper. The magnetic field $\mathbf{H}_{\rm inc}$ can be derived through Maxwell's equations. In our calculations, the background is water with refractive index $n = 1.33$, the incident angle is $\alpha = 55^\circ$, and the nanoparticle with the inner and outer radii $R_1 = 35$ nm and $R_2 = 43$ nm is located at the x axis with $x = 52$ nm except otherwise stated.

The Fano-like resonance-induced left-handed optical torque can be demonstrated by the optical torque as a function of the incident wavelength λ based on the full-wave calculation, which combines the generalized Lorenz-Mie theory with the Maxwell stress tensor approach (see Appendix A). Left-handed optical torque refers to a torque whose direction is opposite with that of the incident angular momentum. The calculated optical torque and incident angular momentum density (given in Appendix B) are presented in Fig. 2 together with the total and partial extinction efficiency $Q_{\rm ext}$. Particle in the interference optical field is only subjected to the optical torque in y direction, viz. T_y discussed in this paper. As the incident frequency increases, the Fano-like resonance comes into play, resulting in the left-handed optical torque near the Fano dip around $\lambda = 463$ nm. The Fano-like resonance is visualized in Fig. 2(b) the total as well as partial extinction efficiency spectra with respect to the incident wavelength λ. For a general isotropic spherical particle, the extinction efficiency can be calculated according to [58,59]

$$Q_{\rm ext} = \sum_{n=1}^{N} (Q_{\rm an} + Q_{\rm bn}), \tag{3}$$

with

$$Q_{\rm an} = \frac{4}{(kR)^2} \sum_{m=-n}^{n} {\rm Re}(|p_{m,n}|^2 a_n),$$

$$Q_{\rm bn} = \frac{4}{(kR)^2} \sum_{m=-n}^{n} {\rm Re}(|q_{m,n}|^2 b_n), \tag{4}$$

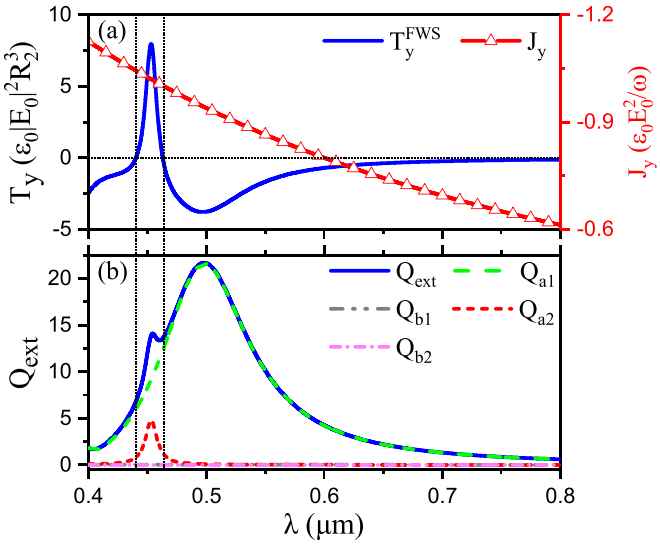

FIG. 2. (a) The y component of the optical torque T_y^{FWS} (solid blue line) and corresponding angular momentum density J_y with details given in Appendix B (solid red line with triangle symbol) as functions of the incident wavelength λ. Left-handed optical torque with direction opposite to that of the angular momentum is induced when an appropriate incident optical wave with $\lambda = 441$ nm to $\lambda = 463$ nm is adopted. (b) The total extinction efficiency Q_{ext} as well as partial extinction efficiencies Q_{an} and Q_{bn}, suggesting that the left-handed optical torque is strongly associated with the Fano-like resonance. The overlap of the broad electric dipole mode with the narrow electric quadrupole mode leads to the appearance of a narrow asymmetric Fano dip at $\lambda = 463$ nm, around which the left-handed optical torque is induced. All other parameters are the same as those in Fig. 1.

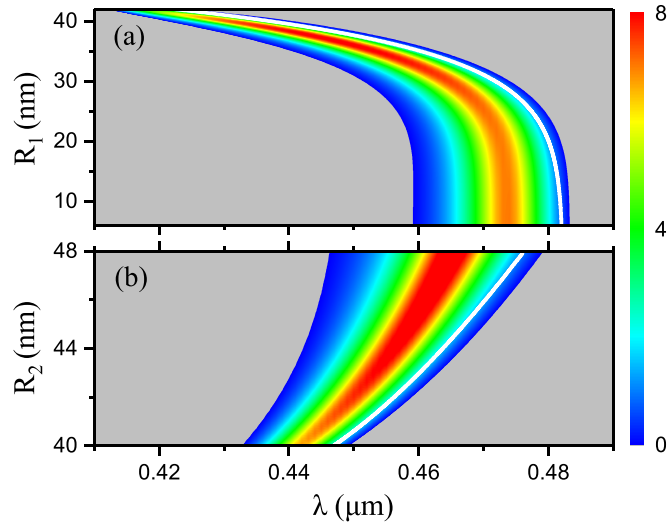

FIG. 3. Phase diagrams of the optical torque T_y^{FWS} in units of $\varepsilon_0|E_0|^2R_2^3$ with respect to the incident wavelength λ as well as the core radius R_1 (a) and shell radius R_2 (b) of the Ag-Au core-shell particle with fixed $R_2 = 43$ nm (a) and $R_1 = 35$ nm (b), respectively. All other parameters are the same as those in Fig. 1. Gray regions indicate the parameter space for the right-handed optical torque phase, while colored regions denote the parameter space to achieve the left-handed optical torque phase. The white line denotes the positions of the Fano dip arising from the interference between the electric dipole and quadrupole modes, which may serve roughly as a guide to the eyes for the onset of the left-handed optical torque phase.

where a_n and b_n are Mie coefficients associated with, respectively, the electric and magnetic multipolar modes [58], ($p_{m,n}$, $q_{m,n}$) are the expansion coefficients of the incident optical field in terms of vector spherical wave function [60], while $R = R_2$ is the particle radius. For small particle with $R \ll \lambda$ in the range from 463 to 800 nm, the total extinction spectra, as shown in Fig. 2(b) by solid blue line, is dominant by the contribution from the electric dipole mode denoted by the dashed green line. The corresponding optical torque in this range is right-handed sharing the same direction with the incident angular momentum density, as presented in Fig. 2(a). With the decrease of the wavelength, the contribution from electric quadrupole mode is brought into play, as shown by the dotted red line. The Fano-like resonance between the broad electric dipole mode (bright mode) and the narrow electric quadrupole mode (dark mode) is therefore enhanced around the electric quadrupole resonance, which gives rise to the left-handed optical torque. As the incident wavelength decreases further to smaller than $\lambda = 441$ nm, the Fano-like resonance disappears due to the vanishing narrow electric quadrupole mode, and then right-handed optical torque is induced instead of the left-handed one. Therefore, when an appropriate incident beam is adopted, viz. with the incident wavelength in the range of 441 to 463 nm in our case, the left-handed optical torque will occur, which stems from the electric dipole-quadrupole Fano-like resonance.

The Fano-like resonance-induced left-handed optical torque presents the flexible adjustability as the same as corresponding Fano resonance-induced negative optical force [49,52], which originates from the flexible tailored Fano-like resonance by particle properties such as particle size, shape and composition. A typical example is shown in Fig. 3 by demonstrating the phase diagrams of optical torque T_y^{FWS} versus incident wavelength λ and core radius R_1 (a) as well as shell radius R_2 (b) for an Ag-Au particle with fixed shell radius $R_2 = 43$ nm (a) and core radius $R_1 = 35$ nm (b), respectively. The parameter spaces corresponding to left- and right-handed optical torques can be discerned by the colored and gray regions in Fig. 3. The Fano dip corresponding to the Ag-Au core-shell particle with different parameter configuration is marked by the white line closed to the low-frequency side of the colored left-handed optical torque phase. The crucial role of Fano-like resonance in inducing left-handed optical torque is therefore suggested, in good agreement with Fig. 2. It can also be observed in Fig. 3 that the left-handed optical torque phase shrinks and exhibits a blue shift as the core Ag radius increases, while the increasing of the Au shell radius leads to a red shift of the left-handed optical torque phase, consistent with the tendency of the Fano dip. These size-induced shifts originate physically from the hybridized coupling plasmon resonances between the Ag core and the Au shell, as it will be discussed in later text.

To understand the essential mechanism of the left-handed optical torque, we first derive an analytical expression of optical torque based on the multipole expansion theory up to

electric quadrupole (detailed in Appendix C)

$$\langle \mathbf{T} \rangle = \mathbf{T}_{\mathrm{e}} + \mathbf{T}_{\mathrm{ee}} + \mathbf{T}_{\mathrm{m}} + \mathbf{T}_{\mathrm{mm}} + \mathbf{T}_{\mathrm{Q^e}} + \mathbf{T}_{\mathrm{Q^eQ^e}}, \tag{5}$$

with

$$\begin{aligned}
\mathbf{T}_{\mathrm{e}} &= \frac{1}{2}\,\mathrm{Re}\,(\mathbf{p} \times \mathbf{E}^*_{\mathrm{inc}}),\\
\mathbf{T}_{\mathrm{ee}} &= \frac{k^3}{12\pi\varepsilon_0}\,\mathrm{Im}\,(\mathbf{p} \times \mathbf{p}^*),\\
\mathbf{T}_{\mathrm{m}} &= \frac{1}{2}\,\mathrm{Re}\,(\mathbf{m} \times \mathbf{B}^*_{\mathrm{inc}}),\\
\mathbf{T}_{\mathrm{mm}} &= \frac{\mu_0 k^3}{12\pi}\,\mathrm{Im}\,(\mathbf{m} \times \mathbf{m}^*),\\
\mathbf{T}_{\mathrm{Q^e}} &= \frac{1}{4}\,\mathrm{Re}[(\nabla \mathbf{E}^*_{\mathrm{inc}}) \cdot \overleftrightarrow{\mathbf{Q}} - \overleftrightarrow{\mathbf{Q}} \cdot (\nabla \mathbf{E}^*_{\mathrm{inc}})] \overset{(2)}{:} \overleftrightarrow{\boldsymbol{\epsilon}},\\
\mathbf{T}_{\mathrm{Q^eQ^e}} &= -\frac{k^5}{80\pi\varepsilon_0}\,\mathrm{Im}[\overleftrightarrow{\mathbf{Q}} \cdot \overleftrightarrow{\mathbf{Q}}^*] \overset{(2)}{:} \overleftrightarrow{\boldsymbol{\epsilon}},
\end{aligned} \tag{6}$$

where ε_0 and μ_0 denote the permittivity and permeability in background, $\mathbf{E}_{\mathrm{inc}}$ and $\mathbf{B}_{\mathrm{inc}}$ are the incident fields given in Eq. (1), $\mathbf{p}$, $\mathbf{m}$, and $\overleftrightarrow{\mathbf{Q}}$ represent, respectively, electric dipole, magnetic dipole, and electric quadrupole moments excited in the particle. The $\overset{(2)}{:}$ is the double contraction between two tensors of ranks, and $\overleftrightarrow{\boldsymbol{\epsilon}}$ denotes the Levi-Civita tensor. $\mathbf{T}_{\mathrm{e}}$, $\mathbf{T}_{\mathrm{m}}$, and $\mathbf{T}_{\mathrm{Q^e}}$ all originate from the interaction between the incident optical field and multipoles excited in the particle, which can be physically understood from the procedure that light is intercepted by the particle. $\mathbf{T}_{\mathrm{ee}}$, $\mathbf{T}_{\mathrm{mm}}$, and $\mathbf{T}_{\mathrm{Q^eQ^e}}$ come from the coupling between various multipoles with the same type, interpreted from the process that light is re-emitted by the multipoles excited in the particle. The reliability of analytical formulation derived within the multipole expansion theory can be examined by the full-wave calculation result due to its high precision. As shown in Fig. 4, the T_y^{FWS} presented in Fig. 2(a) is reproduced by T_y calculated with Eqs. (5) and (6), verifying the accuracy of analytical expressions of optical torque.

To reveal the underlying physics behind the left-handed optical torque more specifically, the optical torque T_y is further decomposed into terms depicting interaction between incident field and multipoles as well as coupling between various multipoles, collectively referred to as different coupling channels here. For clarity, T_{m}^y and T_{mm}^y arising from coupling channels associated with magnetic dipole are neglected in Fig. 4 since they have no contribution to the total optical torque. In the Rayleigh regime where particle size is much smaller than the illuminating wavelength, no optical torque is induced, since the T_{e}^y and T_{ee}^y from the lowest two coupling channels regarding electric dipole almost have the identical amplitude but opposite direction, canceling each other. As the wavelength decreases, the amplitude of T_{e}^y coming from electric dipole-incident electric field coupling channel gradually surpasses T_{ee}^y arising from electric dipole-electric dipole coupling channel, giving rise to a finite but still relatively insignificant right-handed optical torque. A further decrease of the incident wavelength brings about the excitation of the electric quadrupole mode, thus opening the coupling channel between the electric quadrupole and the incident electric field

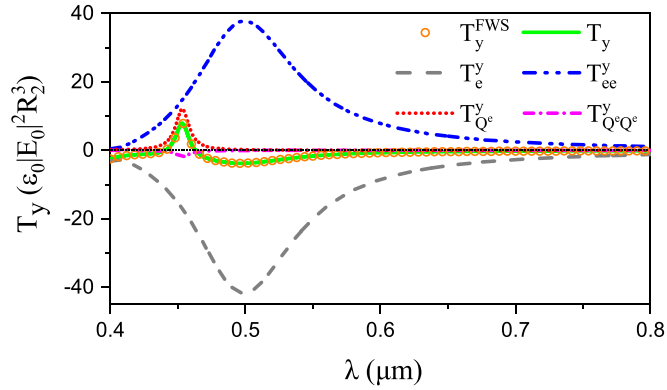

FIG. 4. The optical torque calculated by the multipole expansion theory is denoted by T_y, while T_y^{FWS} computed by the full-wave calculation given in Fig. 2 is also reproduced here. The perfect agreement between T_y and T_y^{FWS} verify the reliability of the multipolar expansion theory of optical torque. Also shown are constituent terms of T_y originating from different coupling channels, specifically, T_{e}^y and T_{ee}^y from the lowest two coupling channels regarding electric dipole while $T_{\mathrm{Q^e}}^y$ and $T_{\mathrm{Q^eQ^e}}^y$ from interaction concerning electric quadrupole. Both T_{m}^y and T_{mm}^y give no contribution to the T_y and thus are not demonstrated here for clarity. All the parameters are the same as those in Fig. 2.

which contributes to $T_{\mathrm{Q^e}}^y$, leading to a reversal of the optical torque from right-hand to left-hand in the visible light spectrum ranging from 441 to 463 nm. The physical origin of the left-handed optical torque can be therefore thoroughly traced to the interaction between the electric quadrupole and the incident electric field, which is associated with the Fano-like resonance presented in Fig. 2(b).

We next turn to the corresponding contribution of a naked Ag core and an Au shell to left-handed optical torque on the core-shell Ag-Au particle. Figures 5(a) and 5(c) present the optical torques for the naked Ag core and the hollow Au shell, respectively. The corresponding spectra of extinction efficiencies are also shown, respectively, in Figs. 5(b) and 5(d). The radius of the naked Ag core is 35 nm and the inner and outer radii of the hollow Au shell are 35 and 43 nm, respectively, so that when the Ag core is put inside of the Au shell, they form the Ag-Au core-shell particle discussed. The results for the naked Ag core are quite similar to those shown in Figs. 4 and 2(b), except for a larger left-handed optical torque, which, however, occurs in the ultraviolet band, beyond the conventional range of operating wavelength for optical tweezers. By coating an Au shell that has the lower frequencies of resonances, see, Figs. 5(c) and 5(d), the excitation wavelength for the electric quadrupole can be moved to the visible light band for the core-shell particle, see, Figs. 4 and 2(b), in favor of the experimental implementation. This is because of the hybridization of the different modes from the Ag core and the Au shell. The interaction between the two different plasmon modes can be visually understood with the plasmon hybridization method in Ref. [61].

The emergence of Fano-like resonance-induced left-handed optical torque on core-shell nanoparticles due to the high-order electric quadrupole coupling channels can be once again confirmed by the phase diagrams of decomposed

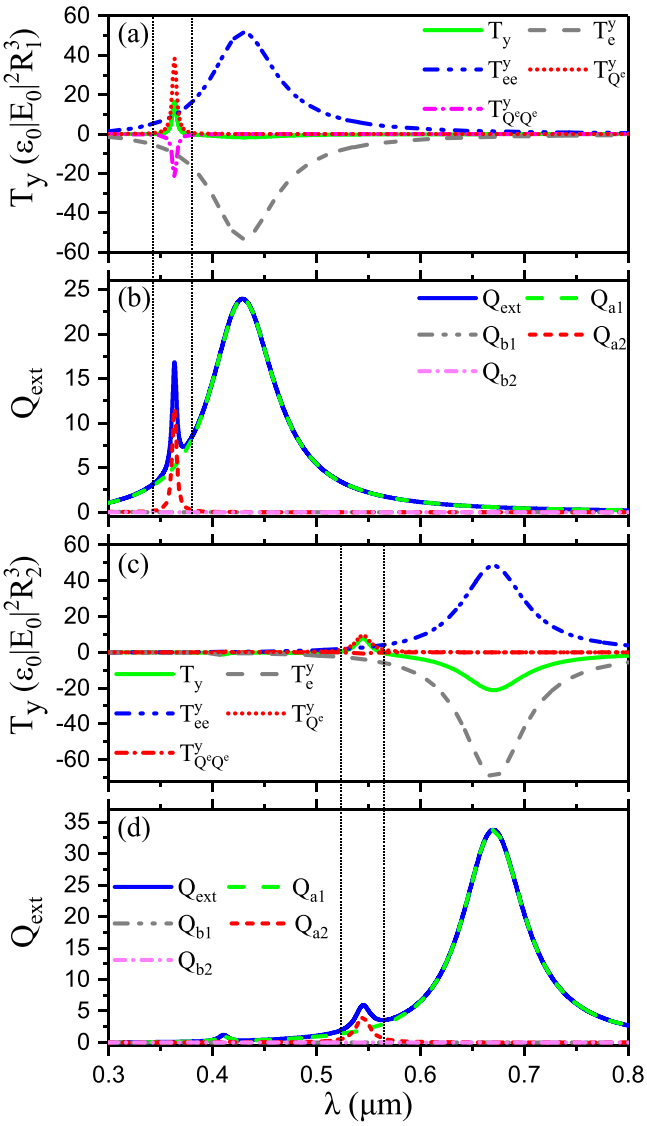

FIG. 5. The optical torque T_y for a naked Ag core with radius $R_1 = 35$ nm (a) and for a hollow Au shell particle with its empty core radius $R_1 = 35$ nm and shell radius $R_2 = 43$ nm (c). Corresponding total extinction efficiencies Q_{ext} as well as partial extinction efficiencies Q_{an} and Q_{bn} are also shown in (b) and (d), respectively. All parameters are the same as those in Fig. 1.

optical torques. The results are presented in Figs. 6(a), 6(c) and 6(b), 6(d) respectively, corresponding to the contribution from low-order dipole coupling channels $T_{dip}^y = T_e^y + T_{ee}^y$ and high-order electric quadrupole coupling channels $T_{quad}^y = T_{Q^e}^y + T_{Q^eQ^e}^y$. One can observe that T_{dip}^y always presents right-handed contribution to the total optical torque in the whole parameter spaces with the variant Ag-Au core-shell nanoparticles as well as incident wavelength, while T_{quad}^y, on the contrary, always demonstrates left-handed contribution. It is T_{quad}^y arising from the high-order electric quadrupole coupling channels that plays the crucial role to give rise to the left-handed optical torque, while this term is dramatically enhanced at the Fano-like resonance, as shown by the solid white line in Figs. 6(b) and 6(d), and thus finally induces the total

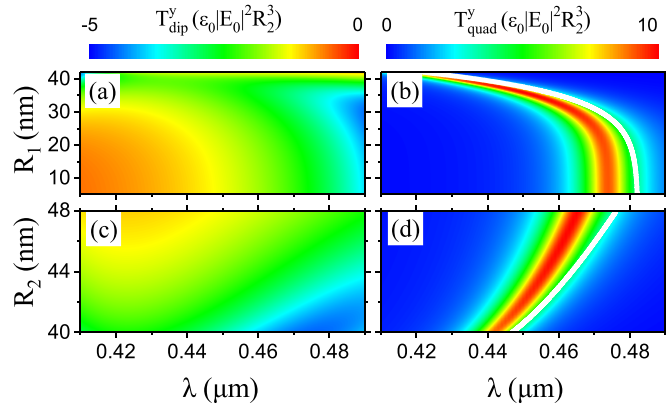

FIG. 6. The decomposed contribution from low-order dipole coupling channels $T_{dip}^y = T_e^y + T_{ee}^y$ (a) (c) and high-order electric quadrupole coupling channels $T_{quad}^y = T_{Q^e}^y + T_{Q^eQ^e}^y$ (b) (d) for the total optical torque T_y^{FWS} as shown in Fig. 3. All parameters are the same as those in Fig. 3.

left-handed optical torque, as shown by the colored region in Figs. 3(a) and 3(b). As a result, the Fano-like resonance due to the simultaneous excitation of multiple multipoles, especially the high-order electric quadrupole, offers a great chance to achieve a left-handed optical torque, adding an additional degree of freedom to optical manipulation of plasmonic nanoparticles.

III. CONCLUSIONS

In summary, we demonstrate that Fano-like resonance can provide an effective way to induce the left-handed optical torque on plasmonic nanoparticles in a simple optical field formed by two interfering plane waves, based on both the numerical full-wave calculation and theoretical multipole expansion technique. The extinction spectra indicate that the Fano-like resonance can be attributed to the coupling between the electric broad dipole mode and narrow quadrupole mode, which can be engineered by tuning the particle composition and operating wavelength, finally giving rise to the flexibly controlled left-handed optical torque. Based on the analytical expressions of optical torque up to electric quadrupole term, the physical origin of the left-handed optical torque can be thoroughly traced to the contribution from the coupling channel of the high-order electric quadrupole, while the low-order dipole coupling channels always give the right-handed optical torque, destroying the scenery of the left-handed optical torque. It should be noted that two plane waves are the simplest illumination to obtain a left-handed optical torque in our situation, since the optical torque in a single plane wave always share the same sign with the incident angular momentum density. Our results may add an additional degree of freedom to realize left-handed optical torque as well as extend the applications of the Fano-like resonance existing widely in many scientific fields.

ACKNOWLEDGMENTS

This work was supported by Natural Science Foundation of Guangxi Province (2021GXNSFDA196001), National Natural Science Foundation of China (12174076 and 12074084),

and Open Project of State Key Laboratory of Surface Physics in Fudan University (KF2019_11).

APPENDIX A: OPTICAL TORQUE BY FULL-WAVE CALCULATION

Based on the generalized Mie scattering theory and the Maxwell stress tensor [62–64], we can obtain the optical torque exerted on a spherical particle by integrating the time-averaged Maxwell stress tensor over a closed surface surrounding the particle [65]

$$\langle \mathbf{T} \rangle = -\oint_S \mathbf{n} \cdot [\langle \overleftrightarrow{\mathbf{T}} \rangle \times \mathbf{r}] d\sigma = \oint_S \mathbf{r} \times [\langle \overleftrightarrow{\mathbf{T}} \rangle \cdot \mathbf{n}] d\sigma, \quad \text{(A1)}$$

the time averaged Maxwell stress tensor $\langle \overleftrightarrow{\mathbf{T}} \rangle$ is given by [1,62,63]

$$\langle \overleftrightarrow{\mathbf{T}} \rangle = \frac{1}{2} \mathrm{Re}\left[\varepsilon_0 \mathbf{E}\mathbf{E}^* + \mu_0 \mathbf{H}\mathbf{H}^* - \frac{1}{2}(\varepsilon_0 \mathbf{E} \cdot \mathbf{E}^* + \mu_0 \mathbf{H} \cdot \mathbf{H}^*) \overleftrightarrow{\mathbf{I}}\right], \quad \text{(A2)}$$

where the permittivity and permeability of the background medium represent as ε_0 and μ_0, respectively. The superscript symbol $*$ denotes the complex conjugate, and the total electromagnetic fields $\mathbf{E}$ and $\mathbf{H}$ can be obtained from the generalized Mie scattering theory. Due to the conservation of momentum, the integral can be implemented at infinity for a particle in the lossless background medium. After some complicated mathematical derivation, three Cartesian components of the optical torque can be expressed as [19]

$$T_x = \mathrm{Re}\,[T_1], \quad T_y = \mathrm{Im}\,[T_1], \quad T_z = \mathrm{Re}\,[T_2], \quad \text{(A3)}$$

with

$$T_1 = \frac{2\pi\varepsilon_0 E_0^2}{k^3} \sum_{n,m} \left[\frac{(n-m)(n+m+1)}{n^2(n+1)^2}\right]^{1/2} t_1,$$

$$T_2 = -\frac{2\pi\varepsilon_0 E_0^2}{k^3} \sum_{n,m} m\, t_2, \quad \text{(A4)}$$

where k is the wave number in the background and

$$t_1 = a_{m,n} a^*_{m+1,n} + b_{m,n} b^*_{m+1,n} - \frac{1}{2}(a_{m,n} p^*_{m+1,n} + p_{m,n} a^*_{m+1,n} + b_{m,n} q^*_{m+1,n} + q_{m,n} b^*_{m+1,n}),$$

$$t_2 = a_{m,n} a^*_{m,n} + b_{m,n} b^*_{m,n} - \frac{1}{2}(a_{m,n} p^*_{m,n} + p_{m,n} a^*_{m,n} + b_{m,n} q^*_{m,n} + q_{m,n} b^*_{m,n}). \quad \text{(A5)}$$

In Eq. (A5), $a_{m,n}$ and $b_{m,n}$ are expansion coefficients of the scattered field in terms of vector spherical wave functions, which are associated with the expansion coefficients of the incident field $p_{m,n}$ and $q_{m,n}$ [60],

$$a_{m,n} = a_n p_{m,n}, \quad b_{m,n} = b_n q_{m,n}, \quad \text{(A6)}$$

where Mie coefficients a_n and b_n describe the scattering property of a conventional isotropic spherical particle. For a core-shell sphere, a_n and b_n can be obtained by [58]

$$a_n = \frac{\psi_n(y)[\psi_n'(m_2 y) - A_n \chi_n'(m_2 y)] - m_2 \psi_n'(y)[\psi_n(m_2 y) - A_n \chi_n(m_2 y)]}{\xi_n(y)[\psi_n'(m_2 y) - A_n \chi_n'(m_2 y)] - m_2 \xi_n'(y)[\psi_n(m_2 y) - A_n \chi_n(m_2 y)]},$$

$$b_n = \frac{m_2 \psi_n(y)[\psi_n'(m_2 y) - B_n \chi_n'(m_2 y)] - \psi_n'(y)[\psi_n(m_2 y) - B_n \chi_n(m_2 y)]}{m_2 \xi_n(y)[\psi_n'(m_2 y) - B_n \chi_n'(m_2 y)] - \xi_n'(y)[\psi_n(m_2 y) - B_n \chi_n(m_2 y)]}, \quad \text{(A7)}$$

with

$$A_n = \frac{m_2 \psi_n(m_2 x)\psi_n'(m_1 x) - m_1 \psi_n'(m_2 x)\psi_n(m_1 x)}{m_2 \chi_n(m_2 x)\psi_n'(m_1 x) - m_1 \chi_n'(m_2 x)\psi_n(m_1 x)},$$

$$B_n = \frac{m_2 \psi_n(m_1 x)\psi_n'(m_2 x) - m_1 \psi_n(m_2 x)\psi_n'(m_1 x)}{m_2 \psi_n(m_1 x)\chi_n'(m_2 x) - m_1 \chi_n(m_2 x)\psi_n'(m_1 x)},$$

where $\psi_n(z) = z j_n(z)$, $\chi_n(z) = z y_n(z)$, and $\xi_n(z) = -z h_n^{(1)}(z)$ denote Riccati-Bessel functions of the first, second and third kinds, respectively, and $x = kR_1$ and $y = kR_2$ with R_1 and R_2 being the inner and outer radii of the particle. m_1 and m_2 are relative refractive indices of the core and shell relative to the background medium. It should be noted that the Mie coefficients in Eq. (A7) can reduce to those of a homogenous sphere if $m_1 = m_2$.

APPENDIX B: ANGULAR MOMENTUM DENSITY

The total angular momentum density of a monochromatic electromagnetic wave can be expressed as a sum of spin angular momentum density $\mathbf{S}$ [66–69] and orbital angular momentum density $\mathbf{L}$ [65,70]

$$\mathbf{J} = \mathbf{S} + \mathbf{L}, \quad \text{(B1)}$$

with

$$\mathbf{S} = \frac{1}{4\omega} \mathrm{Im}\,[\varepsilon_0 \mathbf{E}^*_{\mathrm{inc}} \times \mathbf{E}_{\mathrm{inc}} + \mu_0 \mathbf{H}^*_{\mathrm{inc}} \times \mathbf{H}_{\mathrm{inc}}],$$

$$\mathbf{L} = \mathbf{r} \times \mathbf{M}, \quad \text{(B2)}$$

and $\mathbf{M}$ being the orbital (canonical) linear momentum density

$$\mathbf{M} = \frac{1}{4\omega} \mathrm{Im}\,[\varepsilon_0 (\nabla \mathbf{E}_{\mathrm{inc}}) \cdot \mathbf{E}^*_{\mathrm{inc}} + \mu_0 (\nabla \mathbf{H}_{\mathrm{inc}}) \cdot \mathbf{H}^*_{\mathrm{inc}}], \quad \text{(B3)}$$

where ω denotes the angular frequency and $\mathbf{r}$ is position vector.

APPENDIX C: OPTICAL TORQUE BY MULTIPOLE EXPANSION TECHNIQUE

For a general particle, the optical torque can be obtained from Eqs. (A1) and (A2). $\mathbf{E}$ and $\mathbf{H}$ in the time averaged Maxwell stress tensor Eq. (A2) are total electromagnetic fields, namely, the sum of the incident $\mathbf{E}_{\mathrm{inc}}$ ($\mathbf{H}_{\mathrm{inc}}$) and the scattered fields $\mathbf{E}_{\mathrm{sca}}$ ($\mathbf{H}_{\mathrm{sca}}$), given by

$$\mathbf{E} = \mathbf{E}_{\mathrm{sca}} + \mathbf{E}_{\mathrm{inc}} \quad \text{and} \quad \mathbf{H} = \mathbf{H}_{\mathrm{sca}} + \mathbf{H}_{\mathrm{inc}}. \quad \text{(C1)}$$

Based on the angular spectrum representation [71], any monochromatic incident fields in source-free region can be expanded in terms of plane waves as

$$\mathbf{E}_{\rm inc} = \oint_{4\pi} \mathbf{e_u}\, e^{ik\mathbf{u}\cdot\mathbf{r}}\, d\Omega_u,$$
$$\mathbf{H}_{\rm inc} = \frac{1}{Z_0}\oint_{4\pi} \mathbf{h_u}\, e^{ik\mathbf{u}\cdot\mathbf{r}}\, d\Omega_u, \tag{C2}$$

where Z_0 is the wave impedance in the background, $\mathbf{u}$ is the real unit vector denoting local direction, while $\mathbf{e_u}$ and $\mathbf{h_u}$ denote the complex vectors amplitudes of plane wave components. It follows from the Maxwell equations that

$$\mathbf{u}\cdot\mathbf{e_u} = 0, \quad \mathbf{u}\cdot\mathbf{h_u} = 0, \quad \mathbf{h_u} = \mathbf{u}\times\mathbf{e_u},$$
$$\mathbf{e_u} = \mathbf{h_u}\times\mathbf{u}, \quad \mathbf{e_u}\cdot\mathbf{h_u} = 0. \tag{C3}$$

The scattered fields at large distance from the scatterer read [72]

$$\mathbf{E}_{\rm sca} = \left(\mathbf{a_n} + \frac{\mathbf{n}\,\alpha_\mathbf{n}}{kr}\right)\frac{e^{ikr}}{kr},$$
$$\mathbf{H}_{\rm sca} = \frac{1}{Z_0}\left(\mathbf{b_n} + \frac{\mathbf{n}\,\beta_\mathbf{n}}{kr}\right)\frac{e^{ikr}}{kr}, \tag{C4}$$

where $\mathbf{n} = \mathbf{r}/r$, the scalars $\alpha_\mathbf{n}$ and $\beta_\mathbf{n}$ depict the longitudinal scattered field components while the vectors $\mathbf{a_n}$ and $\mathbf{b_n}$ characterize the transverse amplitudes of the fields. The Maxwell equations yield

$$\mathbf{n}\cdot\mathbf{a_n} = 0, \quad \mathbf{n}\cdot\mathbf{b_n} = 0, \quad \mathbf{b_n} = \mathbf{n}\times\mathbf{a_n},$$
$$\mathbf{a_n} = \mathbf{b_n}\times\mathbf{n}, \quad \mathbf{a_n}\cdot\mathbf{b_n} = 0. \tag{C5}$$

Decomposition of the total fields Eq. (C1) suggests that the time averaged Maxwell stress tensor $\langle\overleftrightarrow{\mathbf{T}}\rangle$ can be cast into

$$\langle\overleftrightarrow{\mathbf{T}}\rangle = \langle\overleftrightarrow{\mathbf{T}}_{\rm inc}\rangle + \langle\overleftrightarrow{\mathbf{T}}_{\rm mix}\rangle + \langle\overleftrightarrow{\mathbf{T}}_{\rm sca}\rangle, \tag{C6}$$

where $\langle\overleftrightarrow{\mathbf{T}}_{\rm inc}\rangle$ involves the incident fields only, $\langle\overleftrightarrow{\mathbf{T}}_{\rm sca}\rangle$ depends solely on the scattered fields, while $\langle\overleftrightarrow{\mathbf{T}}_{\rm mix}\rangle$ includes all the rest (mixed) terms. Correspondingly, the optical torque reads

$$\langle\mathbf{T}\rangle = \langle\mathbf{T}_{\rm inc}\rangle + \langle\mathbf{T}_{\rm mix}\rangle + \langle\mathbf{T}_{\rm sca}\rangle, \tag{C7}$$

where

$$\langle\mathbf{T}_{\rm inc}\rangle = -\oint_{S_\infty}\mathbf{n}\cdot[\,\langle\overleftrightarrow{\mathbf{T}}_{\rm inc}\rangle\times\mathbf{r}\,]d\sigma,$$
$$\langle\mathbf{T}_{\rm mix}\rangle = -\oint_{S_\infty}\mathbf{n}\cdot[\,\langle\overleftrightarrow{\mathbf{T}}_{\rm mix}\rangle\times\mathbf{r}\,]d\sigma,$$
$$\langle\mathbf{T}_{\rm sca}\rangle = -\oint_{S_\infty}\mathbf{n}\cdot[\,\langle\overleftrightarrow{\mathbf{T}}_{\rm sca}\rangle\times\mathbf{r}]d\sigma. \tag{C8}$$

According to the angular momentum conservation law [72], $\langle\overleftrightarrow{\mathbf{T}}_{\rm inc}\rangle$ related integration should make no net contribution to the optical torque, viz.

$$\langle\mathbf{T}_{\rm inc}\rangle = -\oint_{S_\infty}\mathbf{n}\cdot[\,\langle\overleftrightarrow{\mathbf{T}}_{\rm inc}\rangle\times\mathbf{r}]d\sigma$$
$$= \oint_{S_\infty}\mathbf{r}\times[\langle\overleftrightarrow{\mathbf{T}}_{\rm inc}\rangle\cdot\mathbf{n}]d\sigma = 0. \tag{C9}$$

The mixed term is, with the use of $\mathrm{Re}[\mathbf{E}_{\rm inc}\mathbf{E}^*_{\rm sca}] = \mathrm{Re}[\mathbf{E}^*_{\rm inc}\mathbf{E}_{\rm sca}]$.

$$\langle\mathbf{T}_{\rm mix}\rangle = -\oint_{S_\infty}\mathbf{n}\cdot[\,\langle\overleftrightarrow{\mathbf{T}}_{\rm mix}\rangle\times\mathbf{r}]d\sigma = \oint_{S_\infty}\mathbf{r}\times[\langle\overleftrightarrow{\mathbf{T}}_{\rm mix}\rangle\cdot\mathbf{n}]d\sigma = \mathbf{T}_1 + \mathbf{T}_2, \tag{C10a}$$

$$\mathbf{T}_1 = \frac{\varepsilon_0}{2}\,\mathrm{Re}\oint_{S_\infty} R_S\,\mathbf{n}\times[(\mathbf{E}^*_{\rm inc}\mathbf{E}_{\rm sca} + \mathbf{E}_{\rm sca}\mathbf{E}^*_{\rm inc})\cdot\mathbf{n}]d\sigma, \tag{C10b}$$

$$\mathbf{T}_2 = \frac{\mu_0}{2}\,\mathrm{Re}\oint_{S_\infty} R_S\,\mathbf{n}\times[(\mathbf{H}^*_{\rm inc}\mathbf{H}_{\rm sca} + \mathbf{H}_{\rm sca}\mathbf{H}^*_{\rm inc})\cdot\mathbf{n}]d\sigma, \tag{C10c}$$

where use has been of $\mathbf{n}\times(\overleftrightarrow{\mathbf{I}}\cdot\mathbf{n}) = \mathbf{n}\times\mathbf{n} = 0$ [73], and $R_S\to\infty$ is the radius of a spherical surface S_∞ enclosing the scatterer.

With Eqs. (C2)–(C5), it follows that

$$\mathbf{T}_1 = \mathbf{T}_1^{(a)} + \mathbf{T}_1^{(b)}, \qquad \mathbf{T}_2 = \mathbf{T}_2^{(a)} + \mathbf{T}_2^{(b)}, \tag{C11a}$$

$$\mathbf{T}_1^{(a)} = \frac{\varepsilon_0}{2k^2}\,\mathrm{Re}\oint_{4\pi} d\Omega_u\,\frac{e^{ikR_S}}{R_S}\oint_{S_\infty}(\mathbf{n}\times\mathbf{e}^*_\mathbf{u})\alpha_\mathbf{n}\,e^{-ikR_S(\mathbf{u}\cdot\mathbf{n})}\,d\sigma_n, \tag{C11b}$$

$$\mathbf{T}_1^{(b)} = \frac{\varepsilon_0}{2k}\,\mathrm{Re}\oint_{4\pi} d\Omega_u\,e^{ikR_S}\oint_{S_\infty}(\mathbf{n}\times\mathbf{a_n})(\mathbf{e}^*_\mathbf{u}\cdot\mathbf{n})\,e^{-ikR_S(\mathbf{u}\cdot\mathbf{n})}\,d\sigma_n, \tag{C11c}$$

$$\mathbf{T}_2^{(a)} = \frac{\varepsilon_0}{2k^2}\,\mathrm{Re}\oint_{4\pi} d\Omega_u\,\frac{e^{ikR_S}}{R_S}\oint_{S_\infty}(\mathbf{n}\times\mathbf{h}^*_\mathbf{u})\beta_\mathbf{n}\,e^{-ikR_S(\mathbf{u}\cdot\mathbf{n})}\,d\sigma_n, \tag{C11d}$$

$$\mathbf{T}_2^{(b)} = \frac{\varepsilon_0}{2k}\,\mathrm{Re}\oint_{4\pi} d\Omega_u\,e^{ikR_S}\oint_{S_\infty}(\mathbf{n}\times\mathbf{b_n})(\mathbf{h}^*_\mathbf{u}\cdot\mathbf{n})\,e^{-ikR_S(\mathbf{u}\cdot\mathbf{n})}\,d\sigma_n. \tag{C11e}$$

Here $\mathbf{n}$ and $\mathbf{u}$ denote the local outward unit normal of the area element $d\sigma_n$ and the solid angle element $d\Omega_u$, respectively. Based on the direct application of Jones Lemma [72], viz.

$$\frac{1}{R_S}\oint_{S_\infty}\mathbf{G}(\mathbf{n})e^{-ikR_S(\mathbf{u}\cdot\mathbf{n})}\,d\sigma_n \sim \frac{2\pi i}{k}[\mathbf{G}(\mathbf{u})e^{-ikR_S} - \mathbf{G}(-\mathbf{u})e^{ikR_S}], \tag{C12}$$

where $\mathbf{G}(\mathbf{n})$ is an arbitrary function of $\mathbf{n}$, whereas $\mathbf{u}$ is an arbitrary real unit vector, and $\mathbf{n}$ is a unit vector in the local outward radial direction of the spherical surface S_∞ with large radius $R_S \to \infty$. By setting $\mathbf{G}(\mathbf{n}) = \alpha_\mathbf{n}\,(\mathbf{n}\times\mathbf{e}_\mathbf{u}^*)$ and $\beta_\mathbf{n}\,(\mathbf{n}\times\mathbf{h}_\mathbf{u}^*)$, respectively, $\mathbf{T}_1^{(a)}$ and $\mathbf{T}_2^{(a)}$ are given by [1,72]

$$\mathbf{T}_1^{(a)} = \frac{\pi\varepsilon_0}{k^3}\,\mathrm{Re}\oint_{4\pi} i\,(\alpha_\mathbf{u} + e^{2ikR_S}\,\alpha_{-\mathbf{u}})(\mathbf{u}\times\mathbf{e}_\mathbf{u}^*)d\Omega_u, \quad \mathbf{T}_2^{(a)} = \frac{\pi\varepsilon_0}{k^3}\,\mathrm{Re}\oint_{4\pi} i\,(\beta_\mathbf{u} + e^{2ikR_S}\,\beta_{-\mathbf{u}})(\mathbf{u}\times\mathbf{h}_\mathbf{u}^*)d\Omega_u. \tag{C13}$$

Due to the absence of $1/R_S$ factor in $\mathbf{T}_1^{(b)}$, one should take into account the higher order terms in the asymptotic expansions of the integration (C11c) [74,75]. Based on the method of stationary phase, it can be derived [74,75] that, instead of Jones's lemma Eq. (C12), we have

$$\oint_{S_\infty} \mathbf{G}(\mathbf{n})e^{-ikR_S(\mathbf{u}\cdot\mathbf{n})}\,d\sigma_n \sim \frac{\pi}{k^2}[e^{-ikR_S}\,\hat{\boldsymbol{L}}^2\mathbf{G}(\mathbf{u}) + e^{ikR_S}\,\hat{\boldsymbol{L}}^2\mathbf{G}(-\mathbf{u})], \tag{C14}$$

if $\mathbf{G}(\mathbf{u}) = \mathbf{G}(-\mathbf{u}) = 0$, where $\hat{\boldsymbol{L}}$ is the angular momentum operator, so that

$$\hat{\boldsymbol{L}}^2 = -\frac{1}{\sin\theta}\,\frac{\partial}{\partial\theta}\left(\sin\theta\,\frac{\partial}{\partial\theta}\right) - \frac{1}{\sin^2\theta}\,\frac{\partial^2}{\partial\phi^2}, \tag{C15}$$

with the Cartesian components of $\mathbf{n}$ given by $(\sin\theta\cos\phi, \sin\theta\sin\phi, \cos\theta)$, and

$$\hat{\boldsymbol{L}}^2\mathbf{G}(\pm\mathbf{u}) = [\hat{\boldsymbol{L}}^2\mathbf{G}(\mathbf{n})]|_{\mathbf{n}=\pm\mathbf{u}}. \tag{C16}$$

By the use of Eq. (C4), the last term is expressed as

$$\begin{aligned}\langle\mathbf{T}_{\mathrm{sca}}\rangle = \mathbf{T}_3 &= \frac{1}{2}\,\mathrm{Re}\oint_{S_\infty} r\,[\varepsilon_0\mathbf{n}\times(\mathbf{E}_{\mathrm{sca}}\mathbf{E}_{\mathrm{sca}}^*\cdot\mathbf{n}) + \mu_0\mathbf{n}\times(\mathbf{H}_{\mathrm{sca}}\mathbf{H}_{\mathrm{sca}}^*\cdot\mathbf{n})]d\sigma_n \\ &= \frac{\varepsilon_0}{2k^3}\,\mathrm{Re}\oint_{4\pi}(\alpha_\mathbf{n}^*\,\mathbf{b}_\mathbf{n} - \beta_\mathbf{n}^*\,\mathbf{a}_\mathbf{n})d\Omega_n,\end{aligned} \tag{C17}$$

then, the optical torque can be represented as

$$\langle\mathbf{T}\rangle = \langle\mathbf{T}_{\mathrm{mix}}\rangle + \langle\mathbf{T}_{\mathrm{sca}}\rangle = \mathbf{T}_1 + \mathbf{T}_2 + \mathbf{T}_3, \tag{C18}$$

where $\langle\mathbf{T}_{\mathrm{sca}}\rangle$ and $\langle\mathbf{T}_{\mathrm{mix}}\rangle$ characterize the recoil torque and the scattering torque, respectively.

We next derive the analytical expression of optical torque up to electric quadrupole shown in Eqs. (5) and (6) in the main text. If the scatterer can be approximated by an electric dipole moment $\mathbf{p}$, a magnetic dipole moment $\mathbf{m}$ and an electric quadrupole moment $\overleftrightarrow{\mathbf{Q}}$, then the scattered fields are given by [76]

$$\begin{aligned}\mathbf{E}_{\mathrm{sca}}(\mathbf{r}) &= \mathbf{G}_1(\mathbf{r})\,\mathbf{p} + \frac{1}{c}\,\mathbf{G}_2(\mathbf{r})\,\mathbf{m} + \mathbf{F}_1(\mathbf{r})\,\mathbf{Q}_\mathbf{n}, \\ \mathbf{H}_{\mathrm{sca}}(\mathbf{r}) &= \frac{1}{Z_0}\left[-\mathbf{G}_2(\mathbf{r})\,\mathbf{p} + \frac{1}{c}\,\mathbf{G}_1(\mathbf{r})\,\mathbf{m} + \mathbf{F}_2(\mathbf{r})\,\mathbf{Q}_\mathbf{n}\right],\end{aligned} \tag{C19}$$

where $\mathbf{n} = \mathbf{r}/r$ and $\mathbf{Q}_\mathbf{n} = \overleftrightarrow{\mathbf{Q}}\cdot\mathbf{n} = \mathbf{n}\cdot\overleftrightarrow{\mathbf{Q}}$ for a symmetric and traceless electric quadrupole moment. The operators $\mathbf{G}_1$, $\mathbf{G}_2$, $\mathbf{F}_1$, and $\mathbf{F}_2$ are given by

$$\begin{aligned}\mathbf{G}_1(\mathbf{r}) &= \frac{e^{ikr}}{4\pi\varepsilon_0 r}\left[k^2(\overleftrightarrow{\mathbf{I}} - \mathbf{n}\,\mathbf{n}) + \frac{1-ikr}{r^2}\,(3\,\mathbf{n}\,\mathbf{n} - \overleftrightarrow{\mathbf{I}})\right]\bullet, \\ \mathbf{G}_2(\mathbf{r}) &= \frac{e^{ikr}}{4\pi\varepsilon_0 r}\,\frac{ik\,(ikr-1)}{r}\,\mathbf{n}\,\times, \\ \mathbf{F}_1(\mathbf{r}) &= \frac{e^{ikr}}{8\pi\varepsilon_0 r}\left[\frac{6 - 6ikr - 3k^2r^2 + ik^3r^3}{r^3}\,(\mathbf{n}\,\mathbf{n} - \overleftrightarrow{\mathbf{I}})\right. \\ &\quad \left. + \frac{9 - 9ikr - 3k^2r^2}{r^3}\,\mathbf{n}\,\mathbf{n}\right]\bullet,\end{aligned}$$

$$\mathbf{F}_2(\mathbf{r}) = \frac{e^{ikr}}{8\pi\varepsilon_0 r}\,\frac{ik(3 - 3ikr - k^2r^2)}{r^2}\,\mathbf{n}\,\times, \tag{C20}$$

where Eqs. (C19) and (C20) are valid anywhere outside of the scatterer. The complex amplitudes $\mathbf{a}_\mathbf{n}$, $\mathbf{b}_\mathbf{n}$, $\alpha_\mathbf{n}$, and $\beta_\mathbf{n}$ for the scattered field Eq. (C4) at large distance from the scatterer are therefore given by

$$\begin{aligned}\mathbf{a}_\mathbf{n} &= \frac{k^3}{4\pi\varepsilon_0}\left[\mathbf{n}\times(\mathbf{p}\times\mathbf{n}) - \frac{1}{c}\,(\mathbf{n}\times\mathbf{m})\right. \\ &\quad \left. - \frac{ik}{2}\,\mathbf{n}\times(\mathbf{Q}_\mathbf{n}\times\mathbf{n})\right] = \mathbf{a}_\mathbf{n}^{(p)} + \mathbf{a}_\mathbf{n}^{(m)} + \mathbf{a}_\mathbf{n}^{(q)}, \\ \mathbf{b}_\mathbf{n} &= \frac{k^3}{4\pi\varepsilon_0}\left[\mathbf{n}\times\mathbf{p} + \frac{1}{c}\,\mathbf{n}\times(\mathbf{m}\times\mathbf{n}) - \frac{ik}{2}\,\mathbf{n}\times\mathbf{Q}_\mathbf{n}\right] \\ &\quad = \mathbf{b}_\mathbf{n}^{(p)} + \mathbf{b}_\mathbf{n}^{(m)} + \mathbf{b}_\mathbf{n}^{(q)} = \mathbf{n}\times\mathbf{a}_\mathbf{n}, \\ \alpha_\mathbf{n} &= -\frac{i\,k^3}{2\pi\varepsilon_0}\,(\mathbf{n}\cdot\mathbf{p}) - \frac{3k^4}{8\pi\varepsilon_0}\,(\mathbf{n}\cdot\mathbf{Q}_n), \\ \beta_\mathbf{n} &= -\frac{i\,k^3}{2\pi\varepsilon_0 c}\,(\mathbf{n}\cdot\mathbf{m}),\end{aligned} \tag{C21}$$

where the electric dipole moment $\mathbf{p}$, magnetic dipole moment $\mathbf{m}$, and electric quadrupole moment $\overleftrightarrow{\mathbf{Q}}$, respectively, can be expressed as [52]

$$\mathbf{p} = \alpha_e\mathbf{E}_{\mathrm{inc}}, \quad \mathbf{m} = \alpha_m\mathbf{B}_{\mathrm{inc}}, \quad \overleftrightarrow{\mathbf{Q}} = \frac{\beta_e}{2}\left(\nabla\mathbf{E}_{\mathrm{inc}} + \nabla\mathbf{E}_{\mathrm{inc}}^{\mathrm{T}}\right), \tag{C22}$$

with $\mathbf{B}_{\rm inc} = \mu_0 \mathbf{H}_{\rm inc}$ and the polarizabilities

$$\alpha_e = \frac{i6\pi\varepsilon_0}{k^3} a_1, \quad \alpha_m = \frac{i6\pi}{\mu_0 k^3} b_1, \quad \beta_e = \frac{i40\pi\varepsilon_0}{k^5} a_2, \tag{C23}$$

where a_1, b_1, and a_2 denote the Mie coefficients [58]. With Eqs. (C17) and (C21), the recoil torque $\langle \mathbf{T}_{\rm sca} \rangle$ is given by

$$\begin{aligned} \langle \mathbf{T}_{\rm sca} \rangle &= \frac{\varepsilon_0}{2k^3} \,\mathrm{Re} \oint_{4\pi} \left(\alpha_{\mathbf{u}}^* \, \mathbf{b}_{\mathbf{u}} - \beta_{\mathbf{u}}^* \, \mathbf{a}_{\mathbf{u}} \right) d\Omega_u \\ &= \frac{k^3}{12\pi\varepsilon_0 c^2} \,\mathrm{Im}[\, \mathbf{m} \times \mathbf{m}^* + c^2 \, \mathbf{p} \times \mathbf{p}^*] + \frac{k^5}{80\pi\varepsilon_0} \,\mathrm{Im}[\, \mathbf{Q}_x \times \mathbf{Q}_x^* + \mathbf{Q}_y \times \mathbf{Q}_y^* + \mathbf{Q}_z \times \mathbf{Q}_z^* \,], \end{aligned} \tag{C24}$$

where $\mathbf{Q}_x = \mathbf{e}_x \cdot \overleftrightarrow{\mathbf{Q}}$, $\mathbf{Q}_y = \mathbf{e}_y \cdot \overleftrightarrow{\mathbf{Q}}$, $\mathbf{Q}_z = \mathbf{e}_z \cdot \overleftrightarrow{\mathbf{Q}}$.

Based on the method of stationary phase, the Eq. (C11) is further derived by first considering the contributions from an electric dipole moment $\mathbf{p}$,

$$\begin{aligned} \mathbf{T}_{1(\mathbf{p})}^{(a)} &= \frac{1}{2} \,\mathrm{Re} \oint_{4\pi} (1 - e^{2ikR_S}) \, (\mathbf{u} \cdot \mathbf{p}) \mathbf{h}_{\mathbf{u}}^* d\Omega_u, \qquad \mathbf{T}_{2(\mathbf{p})}^{(a)} = 0, \\ \mathbf{T}_{1(\mathbf{p})}^{(b)} &= \frac{1}{4} \,\mathrm{Re} \oint_{4\pi} (1 + e^{2ikR_S}) \, (\mathbf{p} \times \mathbf{e}_{\mathbf{u}}^*) d\Omega_u, \\ \mathbf{T}_{2(\mathbf{p})}^{(b)} &= -\frac{1}{4} \,\mathrm{Re} \oint_{4\pi} (1 - e^{2ikR_S}) [(\mathbf{p} \cdot \mathbf{h}_{\mathbf{u}}^*) \mathbf{u} + (\mathbf{u} \cdot \mathbf{p}) \mathbf{h}_{\mathbf{u}}^*] d\Omega_u, \end{aligned} \tag{C25}$$

where we have, for an electric dipole moment $\mathbf{p}$, made use of

$$\mathbf{a}_{\mathbf{n}}^{(p)} = -\frac{k^3}{4\pi\varepsilon_0} \, \mathbf{n} \times (\mathbf{n} \times \mathbf{p}), \quad \mathbf{b}_{\mathbf{n}}^{(p)} = \frac{k^3}{4\pi\varepsilon_0} \, (\mathbf{n} \times \mathbf{p}), \quad \alpha_{\mathbf{n}}^{(p)} = \frac{-i\,k^3}{2\pi\varepsilon_0} \, (\mathbf{n} \cdot \mathbf{p}), \quad \beta_{\mathbf{n}}^{(p)} = 0. \tag{C26}$$

It then follows directly from Eqs. (C25) and (C13) that

$$\left\langle \mathbf{T}_{\rm mix}^{(\mathbf{p})} \right\rangle = \mathbf{T}_{1(\mathbf{p})}^{(a)} + \mathbf{T}_{1(\mathbf{p})}^{(b)} + \mathbf{T}_{2(\mathbf{p})}^{(a)} + \mathbf{T}_{2(\mathbf{p})}^{(b)} = \frac{1}{2} \,\mathrm{Re} \oint (\mathbf{p} \times \mathbf{e}_{\mathbf{u}}^*) d\Omega_u = \frac{1}{2} \,\mathrm{Re}[\, \mathbf{p} \times \mathbf{E}_{\rm inc}^*], \tag{C27}$$

where $\mathbf{T}_{1(\mathbf{p})}^{(a)}$ and $\mathbf{T}_{1(\mathbf{p})}^{(a)}$ are given by plugging in Eqs. (C26) to (C13). Similar to electric dipoles, the magnetic dipolar term of the scattering torque $\langle \mathbf{T}_{\rm mix}^{(\mathbf{m})} \rangle$ can be expressed as

$$\left\langle \mathbf{T}_{\rm mix}^{(\mathbf{m})} \right\rangle = \mathbf{T}_{1(\mathbf{m})}^{(a)} + \mathbf{T}_{1(\mathbf{m})}^{(b)} + \mathbf{T}_{2(\mathbf{m})}^{(a)} + \mathbf{T}_{2(\mathbf{m})}^{(b)} = \frac{1}{2c} \,\mathrm{Re} \oint (\mathbf{m} \times \mathbf{h}_{\mathbf{u}}^*) d\Omega_u = \frac{1}{2} \,\mathrm{Re}[\, \mathbf{m} \times \mathbf{B}_{\rm inc}^*], \tag{C28}$$

where use has been made of

$$\mathbf{a}_{\mathbf{n}}^{(m)} = -\frac{k^3}{4\pi\varepsilon_0 c} \, (\mathbf{n} \times \mathbf{m}), \quad \mathbf{b}_{\mathbf{n}}^{(m)} = -\frac{k^3}{4\pi\varepsilon_0 c} \, \mathbf{n} \times (\mathbf{n} \times \mathbf{m}), \quad \alpha_{\mathbf{n}}^{(m)} = 0, \quad \beta_{\mathbf{n}}^{(m)} = \frac{-i\,k^3}{2\pi\varepsilon_0 c} \, (\mathbf{n} \cdot \mathbf{m}), \tag{C29}$$

for a magnetic dipole moment $\mathbf{m}$. The terms $\mathbf{T}_{1(\mathbf{m})}^{(a)}$ and $\mathbf{T}_{2(\mathbf{m})}^{(a)}$ are obtained by plugging Eq. (C29) into Eq. (C13), while $\mathbf{T}_{1(\mathbf{m})}^{(b)}$ and $\mathbf{T}_{2(\mathbf{m})}^{(b)}$ are given by

$$\begin{aligned} \mathbf{T}_{1(\mathbf{m})}^{(a)} &= 0, \qquad \mathbf{T}_{2(\mathbf{m})}^{(a)} = -\frac{1}{2c} \,\mathrm{Re} \oint_{4\pi} (1 - e^{2ikR_S}) \, (\mathbf{u} \cdot \mathbf{m}) \mathbf{e}_{\mathbf{u}}^* d\Omega_u, \\ \mathbf{T}_{1(\mathbf{m})}^{(b)} &= \frac{1}{4c} \,\mathrm{Re} \oint_{4\pi} (1 - e^{2ikR_S}) [(\mathbf{m} \cdot \mathbf{e}_{\mathbf{u}}^*) \mathbf{u} + (\mathbf{u} \cdot \mathbf{m}) \mathbf{e}_{\mathbf{u}}^*] d\Omega_u, \\ \mathbf{T}_{2(\mathbf{m})}^{(b)} &= \frac{1}{4c} \,\mathrm{Re} \oint_{4\pi} (1 + e^{2ikR_S}) \, (\mathbf{m} \times \mathbf{h}_{\mathbf{u}}^*) d\Omega_u. \end{aligned} \tag{C30}$$

For electric quadrupole moment $\overleftrightarrow{\mathbf{Q}}$, one has

$$\mathbf{a}_{\mathbf{n}}^{(q)} = \frac{i\,k^4}{8\pi\varepsilon_0} \, \mathbf{n} \times (\mathbf{n} \times \mathbf{Q}_{\mathbf{n}}), \quad \mathbf{b}_{\mathbf{n}}^{(q)} = \frac{-i\,c\,k^4}{8\pi} \, \mathbf{n} \times \mathbf{Q}_{\mathbf{n}}, \quad \alpha_{\mathbf{n}}^{(q)} = -\frac{3k^4}{8\pi\varepsilon_0} \, (\mathbf{n} \cdot \mathbf{Q}_{\mathbf{n}}), \quad \beta_{\mathbf{n}}^{(q)} = 0. \tag{C31}$$

Substituting Eq. (C31) into Eqs. (C11) and (C13), we can arrive at

$$\mathbf{T}_{1(\overleftrightarrow{\mathbf{Q}})}^{(a)} = -\frac{3k}{8} \,\mathrm{Re} \oint_{4\pi} i \, (1 + e^{2ikR_S}) (\mathbf{n} \cdot \mathbf{Q}_{\mathbf{n}}) \mathbf{h}_{\mathbf{n}}^* d\Omega_n, \qquad \mathbf{T}_{2(\overleftrightarrow{\mathbf{Q}})}^{(a)} = 0, \tag{C32a}$$

$$\mathbf{T}_{1(\overleftrightarrow{\mathbf{Q}})}^{(b)} = \frac{k}{8} \,\mathrm{Re} \oint_{4\pi} i \, (1 - e^{2ikR_S}) [2 \, \mathbf{e}_{\mathbf{n}}^* \times (\overleftrightarrow{\mathbf{Q}} \cdot \mathbf{n}) + (\mathbf{e}_{\mathbf{n}}^* \times \mathbf{n}) \cdot \overleftrightarrow{\mathbf{Q}}] d\Omega_n \tag{C32b}$$

$$= \frac{k}{8}\,\mathrm{Re}\oint_{4\pi} i\,(1-e^{2ikR_s})[2\,\mathbf{n}\times(\mathbf{e}_\mathbf{n}^*\cdot\overleftrightarrow{\mathbf{Q}})+\mathbf{h}_\mathbf{n}^*\cdot\overleftrightarrow{\mathbf{Q}}]d\Omega_n, \tag{C32c}$$

$$\mathbf{T}^{(b)}_{2(\overleftrightarrow{\mathbf{Q}})} = \frac{k}{8}\,\mathrm{Re}\oint_{4\pi} i\,(1+e^{2ikR_s})[3(\mathbf{n}\cdot\mathbf{Q}_\mathbf{n})\mathbf{h}_\mathbf{n}^*+2\mathbf{n}\times[(\mathbf{h}_\mathbf{n}^*\times\mathbf{n})\cdot\overleftrightarrow{\mathbf{Q}}]+\mathbf{h}_\mathbf{n}^*\cdot\overleftrightarrow{\mathbf{Q}}]d\Omega_n. \tag{C32d}$$

So one has, with $\overleftrightarrow{\boldsymbol{\epsilon}}$ denoting the Levi-Civita antisymmetric tensor of rank 3

$$\langle\mathbf{T}^{(\overleftrightarrow{\mathbf{Q}})}_{\mathrm{mix}}\rangle = \mathbf{T}^{(a)}_{1(\overleftrightarrow{\mathbf{Q}})}+\mathbf{T}^{(b)}_{1(\overleftrightarrow{\mathbf{Q}})}+\mathbf{T}^{(a)}_{2(\overleftrightarrow{\mathbf{Q}})}+\mathbf{T}^{(b)}_{2(\overleftrightarrow{\mathbf{Q}})} = \frac{k}{4}\,\mathrm{Re}\oint_{4\pi} i[\,2\mathbf{u}\times(\mathbf{e}_\mathbf{u}^*\cdot\overleftrightarrow{\mathbf{Q}})+\mathbf{h}_\mathbf{u}^*\cdot\overleftrightarrow{\mathbf{Q}}]d\Omega_u \tag{C33a}$$

$$= \frac{k}{2}\,\mathrm{Re}\oint_{4\pi} i\,u_\alpha(e_\beta^*\mathcal{Q}_{\beta\gamma})\epsilon_{\alpha\gamma\delta}\,d\Omega_n+\frac{k}{4}\,\mathrm{Re}\oint_{4\pi} i\,\mathbf{h}_\mathbf{u}^*\,d\Omega_u\cdot\overleftrightarrow{\mathbf{Q}} \tag{C33b}$$

$$= \frac{1}{2}\,\mathrm{Re}[(\nabla\mathbf{E}_{\mathrm{inc}}^*)\cdot\overleftrightarrow{\mathbf{Q}}]\overset{(2)}{\vdots}\overleftrightarrow{\boldsymbol{\epsilon}}-\frac{\omega}{4}\,\mathrm{Im}[\mathbf{B}_{\mathrm{inc}}^*\cdot\overleftrightarrow{\mathbf{Q}}]. \tag{C33c}$$

The double contraction between two tensors of ranks l and l', denoted by $\overset{(m)}{\vdots}$, is defined below

$$\overleftrightarrow{\mathbb{A}}^{(l)}\overset{(m)}{\vdots}\overleftrightarrow{\mathbb{B}}^{(l')} = \mathbb{A}^{(l)}_{i_1 i_2\cdots i_{l-m}\,k_1 k_2\cdots k_{m-1}\,k_m}\,\mathbb{B}^{(l')}_{k_m k_{m-1}\cdots k_2 k_1\,j_{m+1}\cdots j_{l'-1}\,j_{l'}},\quad 0\leqslant m\leqslant\min[\,l,l'\,], \tag{C34}$$

which yielding a tensor of rank $l+l'-2m$. We can obtain a more symmetric form for the electric quadrupole term of the scattering torque

$$\langle\mathbf{T}^{(\overleftrightarrow{\mathbf{Q}})}_{\mathrm{mix}}\rangle = \frac{1}{4}\,\mathrm{Re}[(\nabla\mathbf{E}_{\mathrm{inc}}^*)\cdot\overleftrightarrow{\mathbf{Q}}-\overleftrightarrow{\mathbf{Q}}\cdot(\nabla\mathbf{E}_{\mathrm{inc}}^*)]\overset{(2)}{\vdots}\overleftrightarrow{\boldsymbol{\epsilon}}. \tag{C35}$$

With Eqs. (C24), (C27), (C28), and (C35), one finally arrives at the multipole expansion of optical torque up to electric quadrupole

$$\langle\mathbf{T}\rangle = \mathbf{T}_\mathrm{e}+\mathbf{T}_\mathrm{ee}+\mathbf{T}_\mathrm{m}+\mathbf{T}_\mathrm{mm}+\mathbf{T}_{\mathrm{Q^e}}+\mathbf{T}_{\mathrm{Q^eQ^e}}, \tag{C36}$$

with

$$\mathbf{T}_\mathrm{e} = \frac{1}{2}\,\mathrm{Re}\,(\mathbf{p}\times\mathbf{E}_{\mathrm{inc}}^*),\qquad \mathbf{T}_\mathrm{ee} = \frac{k^3}{12\pi\varepsilon_0}\,\mathrm{Im}\,(\mathbf{p}\times\mathbf{p}^*),$$

$$\mathbf{T}_\mathrm{m} = \frac{1}{2}\,\mathrm{Re}\,(\mathbf{m}\times\mathbf{B}_{\mathrm{inc}}^*),\qquad \mathbf{T}_\mathrm{mm} = \frac{\mu_0 k^3}{12\pi}\,\mathrm{Im}\,(\mathbf{m}\times\mathbf{m}^*),$$

$$\mathbf{T}_{\mathrm{Q^e}} = \frac{1}{4}\,\mathrm{Re}[(\nabla\mathbf{E}_{\mathrm{inc}}^*)\cdot\overleftrightarrow{\mathbf{Q}}-\overleftrightarrow{\mathbf{Q}}\cdot(\nabla\mathbf{E}_{\mathrm{inc}}^*)]\overset{(2)}{\vdots}\overleftrightarrow{\boldsymbol{\epsilon}},\qquad \mathbf{T}_{\mathrm{Q^eQ^e}} = -\frac{k^5}{80\pi\varepsilon_0}\,\mathrm{Im}[\overleftrightarrow{\mathbf{Q}}\cdot\overleftrightarrow{\mathbf{Q}}^*]\overset{(2)}{\vdots}\overleftrightarrow{\boldsymbol{\epsilon}}. \tag{C37}$$

[1] A. Ashkin, *Optical Trapping and Manipulation of Neutral Particles Using Lasers* (World Scientific, Hackensack, 2006)
[2] D. G. Grier, Nature (London) **424**, 810 (2003).
[3] M. Padgett and R. Bowman, Nat. Photonics **5**, 343 (2011).
[4] D. Gao, W. Ding, M. Nieto-Vesperinas, X. Ding, M. Rahman, T. Zhang, C. Lim, and C.-W. Qiu, Light Sci. Appl. **6**, e17039 (2017).
[5] A. Ashkin, Phys. Rev. Lett. **24**, 156 (1970).
[6] J. Baumgartl, M. Mazilu, and K. Dholakia, Nat. Photonics **2**, 675 (2008).
[7] C. Maher-McWilliams, P. Douglas, and P. Barker, Nat. Photonics **6**, 386 (2012).
[8] A. Ashkin, J. M. Dziedzic, J. E. Bjorkholm, and S. Chu, Opt. Lett. **11**, 288 (1986).
[9] M. L. Juan, M. Righini, and R. Quidant, Nat. Photonics **5**, 349 (2011).
[10] M.-C. Zhong, X.-B. Wei, J.-H. Zhou, Z.-Q. Wang, and Y.-M. Li, Nat. Commun. **4**, 1768 (2013).
[11] J. Chen, J. Ng, Z. Lin, and C. T. Chan, Nat. Photonics **5**, 531 (2011).
[12] A. Dogariu, S. Sukhov, and J. Sáenz, Nat. Photonics **7**, 24 (2013).
[13] H. Li, Y. Cao, L.-M. Zhou, X. Xu, T. Zhu, Y. Shi, C.-W. Qiu, and W. Ding, Adv. Opt. Photon. **12**, 288 (2020).
[14] S. H. Simpson, D. C. Benito, and S. Hanna, Phys. Rev. A **76**, 043408 (2007).
[15] D. Haefner, S. Sukhov, and A. Dogariu, Phys. Rev. Lett. **103**, 173602 (2009).
[16] L. Tong, V. D. Miljković, and M. Käll, Nano Lett. **10**, 268 (2010).
[17] M. Nieto-Vesperinas, Phys. Rev. A **92**, 043843 (2015).
[18] M. Nieto-Vesperinas, Opt. Lett. **40**, 3021 (2015).
[19] H. Chen, W. Lu, X. Yu, C. Xue, S. Liu, and Z. Lin, Opt. Express **25**, 32867 (2017).
[20] Q. Zhang, J. Li, and X. Liu, Phys. Chem. Chem. Phys. **21**, 1308 (2019).
[21] Y. E. Lee, K. H. Fung, D. Jin, and N. X. Fang, Nanophotonics **3**, 343 (2014).
[22] R. Fukuhara, Y. Y. Tanaka, and T. Shimura, Phys. Rev. A **100**, 023827 (2019).

[23] J. Chen, J. Ng, K. Ding, K. H. Fung, Z. Lin, and C. T. Chan, Sci. Rep. **4**, 3612 (2014).
[24] K. Diniz, R. Dutra, L. Pires, N. Viana, H. Nussenzveig, and P. M. Neto, Opt. Express **27**, 5905 (2019).
[25] D. Hakobyan and E. Brasselet, Nat. Photonics **8**, 610 (2014).
[26] H. Magallanes and E. Brasselet, Nat. Photonics **12**, 461 (2018).
[27] N. Sule, Y. Yifat, S. K. Gray, and N. F. Scherer, Nano Lett. **17**, 6548 (2017).
[28] F. Han, J. A. Parker, Y. Yifat, C. Peterson, S. K. Gray, N. F. Scherer, and Z. Yan, Nat. Commun. **9**, 4897 (2018).
[29] A. Canaguier-Durand and C. Genet, Phys. Rev. A **92**, 043823 (2015).
[30] Y.-X. Hu, R.-C. Jin, X.-R. Zhang, L.-L. Tang, J.-Q. Li, J. Wang, and Z.-G. Dong, Opt. Commun. **482**, 126560 (2021).
[31] U. Fano, Phys. Rev. **124**, 1866 (1961).
[32] B. Luk'yanchuk, N. I. Zheludev, S. A. Maier, N. J. Halas, P. Nordlander, H. Giessen, and C. T. Chong, Nat. Mater. **9**, 707 (2010).
[33] A. E. Miroshnichenko, S. Flach, and Y. S. Kivshar, Rev. Mod. Phys. **82**, 2257 (2010).
[34] M. V. Rybin, A. B. Khanikaev, M. Inoue, K. B. Samusev, M. J. Steel, G. Yushin, and M. F. Limonov, Phys. Rev. Lett. **103**, 023901 (2009).
[35] F. Bleckmann, E. Maibach, S. Cordes, T. E. Umbach, K. Meerholz, and S. Linden, Adv. Opt. Mater. **2**, 861 (2014).
[36] C. Wu, A. B. Khanikaev, R. Adato, N. Arju, A. A. Yanik, H. Altug, and G. Shvets, Nat. Mater. **11**, 69 (2012).
[37] Y. Francescato, V. Giannini, and S. A. Maier, ACS Nano **6**, 1830 (2012).
[38] W.-S. Chang, J. B. Lassiter, P. Swanglap, H. Sobhani, S. Khatua, P. Nordlander, N. J. Halas, and S. Link, Nano Lett. **12**, 4977 (2012).
[39] C. Argyropoulos, P.-Y. Chen, F. Monticone, G. D'Aguanno, and A. Alu, Phys. Rev. Lett. **108**, 263905 (2012).
[40] F. Le, D. W. Brandl, Y. A. Urzhumov, H. Wang, J. Kundu, N. J. Halas, J. Aizpurua, and P. Nordlander, ACS Nano **2**, 707 (2008).
[41] V. Giannini, R. Rodríguez-Oliveros, and J. A. Sánchez-Gil, Plasmonics **5**, 99 (2010).
[42] S. Mukherjee, H. Sobhani, J. B. Lassiter, R. Bardhan, P. Nordlander, and N. J. Halas, Nano Lett. **10**, 2694 (2010).
[43] S. Zhang, D. A. Genov, Y. Wang, M. Liu, and X. Zhang, Phys. Rev. Lett. **101**, 047401 (2008).
[44] A. J. Pasquale, B. M. Reinhard, and L. Dal Negro, ACS Nano **5**, 6578 (2011).
[45] Z. Li, T. Shegai, G. Haran, and H. Xu, ACS Nano **3**, 637 (2009).
[46] T. Shegai, S. Chen, V. D. Miljković, G. Zengin, P. Johansson, and M. Käll, Nat. Commun. **2**, 481 (2011).
[47] Q. Zhang and J. J. Xiao, Opt. Lett. **38**, 4240 (2013).
[48] Z. Li, S. Zhang, L. Tong, P. Wang, B. Dong, and H. Xu, ACS Nano **8**, 701 (2014).
[49] H. Chen, S. Liu, J. Zi, and Z. Lin, ACS Nano **9**, 1926 (2015).
[50] T. Cao, L. Mao, D. Gao, W. Ding, and C.-W. Qiu, Nanoscale **8**, 5657 (2016).
[51] D. Gao, R. Shi, Y. Huang, and L. Gao, Phys. Rev. A **96**, 043826 (2017).
[52] H. Chen, Q. Ye, Y. Zhang, L. Shi, S. Liu, Z. Jian, and Z. Lin, Phys. Rev. A **96**, 023809 (2017).
[53] T. Cao and Y. Qiu, Nanoscale **10**, 566 (2018).
[54] H. Chen, Y. Huang, and Y. Huang, Phys. Lett. A **388**, 127075 (2021).
[55] O. Peña-Rodríguez and U. Pal, Nanoscale **3**, 3609 (2011).
[56] P. Drude, Ann. Phys. **306**, 566 (1900).
[57] M. A. Ordal, R. J. Bell, R. W. Alexander, L. L. Long, and M. R. Querry, Appl. Opt. **24**, 4493 (1985).
[58] C. F. Bohren and D. R. Huffman, *Absorption and Scattering of Light by Small Particles* (John Wiley and Sons, New York, 1983).
[59] Y.-l. Xu, Appl. Opt. **36**, 9496 (1997).
[60] G. Gouesbet, Opt. Commun. **283**, 517 (2010).
[61] E. Prodan, C. Radloff, N. J. Halas, and P. Nordlander, Science **302**, 419 (2003).
[62] J. D. Jackson, *Classical Electrodynamics* (John Wiley and Sons, New York, 1999).
[63] A. Zangwill, *Modern Electrodynamics* (Cambridge University Press, New York, 2012).
[64] G. Gouesbet and G. Gréhan, *Generalized Lorenz-Mie Theories*, 2nd ed. (Springer, Berlin, 2017).
[65] Y. K. Jiang, H. J. Chen, J. Chen, J. Ng, and Z. F. Lin, arXiv:1511.08546v3.
[66] L. Allen, S. M. Barnett, and M. J. Padgett, *Optical Angular Momentum* (Institute of Physics Publishing, Bristol and Philadelphia, 2016).
[67] C. Cohen-Tannoudji, J. Dupont-Roc, and G. Grynberg, *Photons and Atoms: Introduction to Quantum Electrodynamics* (John Wiley and Sons, New York, 1989).
[68] M. V. Berry, J. Opt. A: Pure Appl. Opt. **11**, 094001 (2009).
[69] K. Y. Bliokh, A. Y. Bekshaev, and F. Nori, Nat. Commun. **5**, 3300 (2014).
[70] M. Padgett, J. Courtial, and L. Allen, Phys. Today **57**(5), 35 (2004).
[71] N. J. Moore and M. A. Alonso, J. Opt. Soc. Am. A **26**, 2211 (2009).
[72] M. Born and E. Wolf, *Principles of Optics*, 7th ed. (Cambridge U. Press, Cambridge, 1999).
[73] H. C. Chen, *Theory of Electromagnetic Waves: A Coordinate-free Approach* (McGraw-Hill, New York, 1983).
[74] J. Stamnes, *Waves in Focal Regions* (IOP, Bristol, 1986).
[75] R. Wong, *Asymptotic Approximations of Integrals* (Academic Press, Boston, 1989).
[76] T. Lemaire, J. Opt. Soc. Am. A **14**, 470 (1997).